Molecular and Cellular Neuroscience xxx (2010) xxx–xxx

Contents lists available at ScienceDirect

Molecular and Cellular Neuroscience

journal homepage: www.elsevier.com/locate/ymcne

C. elegans multi-dendritic sensory neurons: Morphology and function

Adi Albeg [a], Cody J. Smith [b], Marios Chatzigeorgiou [c], Dror G. Feitelson [d], David H. Hall [e], William R. Schafer [c], David M. Miller III [b], Millet Treinin [a,*]

[a] Department of Medical Neurobiology, Institute for Medical Research – Israel-Canada, Hebrew University – Hadassah Medical School, Jerusalem 91120, Israel
[b] Department of Cell and Developmental Biology and Program in Neuroscience, Vanderbilt University, Nashville, TN 37232-8240, USA
[c] Cell Biology Division, MRC Laboratory of Molecular Biology, Hills Road, Cambridge UK
[d] Department of Computer Science, Hebrew University, Jerusalem 91904, Israel
[e] Department of Neuroscience, Albert Einstein College of Medicine, Bronx, NY 10461, USA

ARTICLE INFO

Article history:
Received 3 June 2010
Revised 2 October 2010
Accepted 13 October 2010
Available online xxxx

Keywords:
C. elegans
Somatosensory system
Nociceptor
Proprioceptor
Behavior
Movement

ABSTRACT

PVD and FLP sensory neurons envelope the body of the *C. elegans* adult with a highly branched network of thin sensory processes. Both PVD and FLP neurons are mechanosensors. PVD is known to mediate the response to high threshold mechanical stimuli. Thus PVD and FLP neurons are similar in both morphology and function to mammalian nociceptors. To better understand the function of these neurons we generated strains lacking them. Behavioral analysis shows that PVD and FLP regulate movement under normal growth conditions, as animals lacking these neurons demonstrate higher dwelling behavior. In addition, PVD—whose thin branches project across the body-wall muscles—may have a role in proprioception, as ablation of PVD leads to defective posture. Moreover, movement-dependent calcium transients are seen in PVD, a response that requires MEC-10, a subunit of the mechanosensory DEG/ENaC channel that is also required for maintaining wild-type posture. Hence, PVD senses both noxious and innocuous signals to regulate *C. elegans* behavior, and thus combines the functions of multiple mammalian somatosensory neurons. Finally, strong mechanical stimulation leads to inhibition of egg-laying, and this response also depends on PVD and FLP neurons. Based on all these results we suggest that noxious signals perceived by PVD and FLP promote an escape behavior consisting of increased speed, reduced pauses and reversals, and inhibition of egg-laying.

Introduction

In mammals, the somatosensory system is responsible for diverse sensory modalities including responses to touch and temperature, maintenance of body posture (proprioception), and the feeling of pain (nociception). These neurons perceive stimuli to the outer layer of the body (skin) or to internal organs (Lumpkin and Caterina, 2007). Nociceptors are an important class of somatosensory neurons perceiving high threshold mechanical stimuli, noxious temperatures, and/or tissue damage. Mammalian nociceptors are typically highly branched with multiple naked sensory dendrites (Caterina and Julius, 1999). Nociceptors showing similar morphology and function are seen in *Drosophila,* providing evidence for conservation of this cell type throughout evolution (Tracey et al., 2003).

C. elegans is a useful model organism with a simple, well-characterized nervous system. The *C. elegans* nervous system has 302 neurons, including sensory neurons that are morphologically similar to somatosensory neurons in having dendritic processes positioned immediately underneath the nematode hypodermis or "skin." These neurons are mechanosensory, enabling the response to low threshold mechanical stimuli (the six touch receptor neurons), to bacteria (PDEs), or having a role in proprioception (DVA) (Chalfie and Sulston, 1981; Sawin et al., 2000; Li et al., 2006).

Comprehensive analysis of *C. elegans* neuroanatomy by electron microscopy demonstrated that most *C. elegans* neurons adopt a simple morphology with few branches (White et al., 1986). Our work, however, revealed that PVD neurons are atypical for the nematode, and display elaborate dendritic branching (Halevi et al., 2002; Oren-Suissa et al., 2010; Smith et al., 2010). PVD was previously shown to mediate the response to high threshold mechanical stimuli and thus functions as a nociceptor (Way and Chalfie, 1989). This function of PVD together with the high complexity of PVD branching and position of PVD branches below the outer envelope of the animal are characteristic of mammalian polymodal nociceptors (Caterina and Julius, 1999). Indeed, recent analysis of PVD activity and function shows that PVD senses both cold temperature and high threshold mechanical stimulation (Chatzigeorgiou et al., 2010). Thus, PVD is similar to mammalian and *Drosophila* polymodal nociceptors in both morphology and function (Tracey et al., 2003).

Here we characterize the structure and the functions of PVD and of a related sensory neuron, FLP. Our results show that PVD and FLP

* Corresponding author. Fax: +972 2 6439736.
E-mail address: millet_t@cc.huji.ac.il (M. Treinin).

1044-7431/$ – see front matter © 2010 Elsevier Inc. All rights reserved.
doi:10.1016/j.mcn.2010.10.001

branches envelope the animal with a dense network of dendritic processes producing non-overlapping sensory fields, with the PVD network restricted to the body and tail regions and FLP branches surrounding the head. We show that both PVD and FLP dendritic branches appear simultaneously during late larval development, although FLP neurons are born in the embryo and PVD neurons arise in the second larval stage. We suggest that noxious signals perceived by these neurons mediate an adult escape behavior consisting of increased speed, reduced reversals and pauses, and inhibition of egg-laying. We also show that PVD branches overlay body muscles with multiple sensory processes and suggest that these branches have a role in proprioception. Thus, side branches of PVD and FLP neurons combine multiple roles, perceiving both noxious and innocuous signals, to promote an escape behavior or to regulate body posture.

Results

PVD and FLP neurons envelop the animal in a complex network of sensory processes

PVD and FLP are both highly branched neurons ((Halevi et al., 2002) and http://www.wormatlas.org/neurons/Individual%20Neurons). Analysis of reporters expressed in PVD but not in FLP shows that PVD branches envelop the entire body of the animal with a dense network of branches, a network that does not cover the head region (Tsalik et al., 2003; Watson et al., 2008). Similar analysis of the organization of FLP branches has been difficult since reporters for FLP branches (*deg-3, des-2,* and *mec-3*) are also expressed in the PVD. Therefore, to examine the organization of FLP branches relative to PVD branches, we used *F49H12.4*:GFP to mark PVD and a *mec-7*:RFP reporter to mark both FLP and PVD. In this two-color animal, RFP marked-processes seen in the head resemble the elaborate network of GFP-expressing PVD branches in the body region posterior to the pharynx (Fig. 1). In addition to confirming that FLP and PVD neurons adopt similar dendritic morphologies, our analysis revealed that these FLP and PVD networks occupy discrete regions and do not overlap (Fig. 1). Thus, side branches of the two FLP neurons (FLPL and FLPR) envelop the head of the animal (left and right sides), whereas the two PVD neurons (PVDL and PVDR) similarly ensheathe the body from the tail up to the head (left and right sides). Overall this analysis suggests that the body of *C. elegans* is surrounded with a dense network of branches emanating from four neurons, each receiving inputs from a distinct sensory field that does not overlap with the sensory fields of the other three neurons.

The complexity of PVD and FLP morphology was unexpected in view of the relative simplicity of other *C. elegans* neurons. Moreover, electron microscopy reconstruction of the *C. elegans* nervous system failed to document the full complexity of FLP morphology and did not reveal any of the PVD side branches (2°, 3° and 4° as described in Fig. 1 (White et al., 1986)). However, reexamination of the archival *C. elegans* serial section prints used in that study for evidence of these branches identified many processes in the position suggested by the GFP reporters. These processes correspond to the dorsal and ventral 4° branches, and sometimes the short 3° processes from which the 4° branches emanate ((Oren-Suissa et al., 2010; Smith et al., 2010) and (Figs. 2B–D)).

The 3° processes are similar in diameter and contents to many other neuronal processes in the nematode (Figs. 2A and B), whereas the 4° processes are distinctly narrower, and almost devoid of internal contents (Figs. 2B–D). Due to their very small caliber, it is difficult to follow the course of 4° processes as they run beneath the body-wall muscles. In favorable circumstances, a 4° process might be observed in three sections in a row. However, at the medial edge of each body-wall muscle quadrant, the 4° branches often turn to run in parallel to the body axis, adjacent to either the dorsal or ventral nerve cords

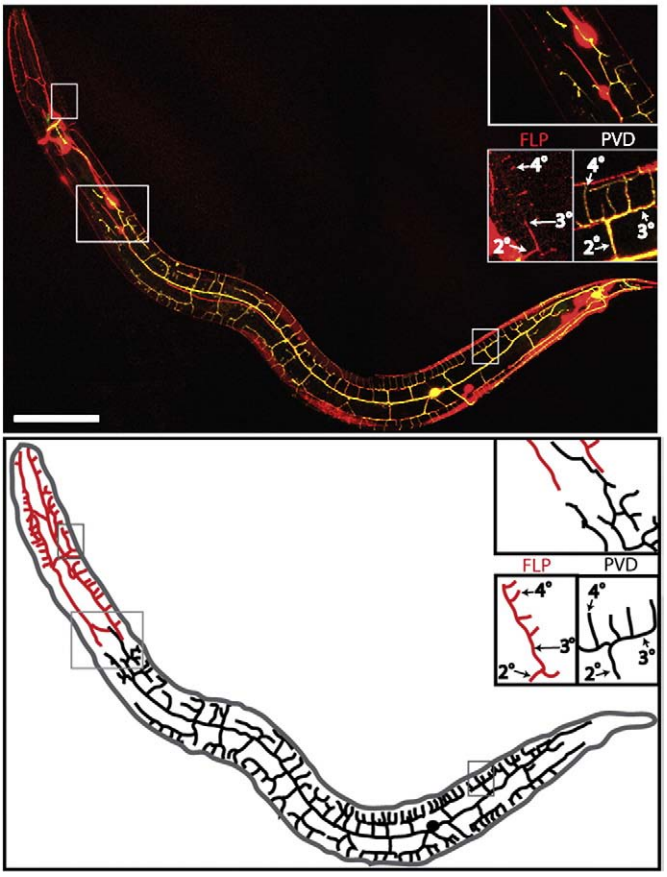

Fig. 1. PVD and FLP branches envelop the nematode's body. Above, confocal reconstruction of an animal expressing *F49H12.4*:GFP (yellow) and *mec-7*:RFP (red). Insets show a representative candelabra-like branching pattern of FLP (head), PVD (body), and a region where PVD and FLP branches meet but do not overlap. Indicated are branch names (2°, 3°, 4°) given according to the order of appearance in development. Below is a line diagram showing PVD (black) and FLP (red) branches. Only processes belonging to either PVD or FLP are shown in this drawing; processes of other neurons expressing either of the two reporters are omitted. Scale bar is 25 μm.

(Fig. 2C). In these areas, the 4° branches can be followed for dozens of serial sections, and indeed some of them were traced by hand by Eileen Southgate and John White and assigned individual "color codes" for local portions (unpublished data from the MRC archive). However, since these processes could not be traced back to their cell of origin, none of these fine processes were included in "Mind of a Worm" (White et al., 1986) and their significance was missed. Interestingly, there are multiple instances where these 4° processes are fused to their nearest neighbors while running along the A/P axis near the nerve cords, thus forming closed loops with neighboring candles in the "candelabra" [indicated in Fig. 2A with arrows] and (Oren-Suissa et al., 2010).

Quaternary (4°) processes tend to retain the same small diameter (35–60 nm) along the entire length of each candle and near a nerve cord. These fine branches are never presynaptic, rarely postsynaptic, and show no evidence (so far) of forming gap junctions. This suggests that their many sensory endings must act in summation to influence distant synaptic relations, rather than in local circuits. The 4° processes always lie in very close association with hypodermis, seemingly separated from the overlying body-wall muscle membrane by the thick basal lamina. Using the head/body boundary to differentiate between PVD and FLP processes (since we still cannot trace them to their cells of origin), the 4° processes of both cell types have the same physical attributes and run in the same locale between the body-wall muscles and the hypodermis. There was no evidence that processes from the left and right cells could interact with their bilateral homologue at either the dorsal or ventral

Please cite this article as: Albeg, A., et al., *C. elegans* multi-dendritic sensory neurons: Morphology and function, Mol. Cell. Neurosci. (2010), doi:10.1016/j.mcn.2010.10.001

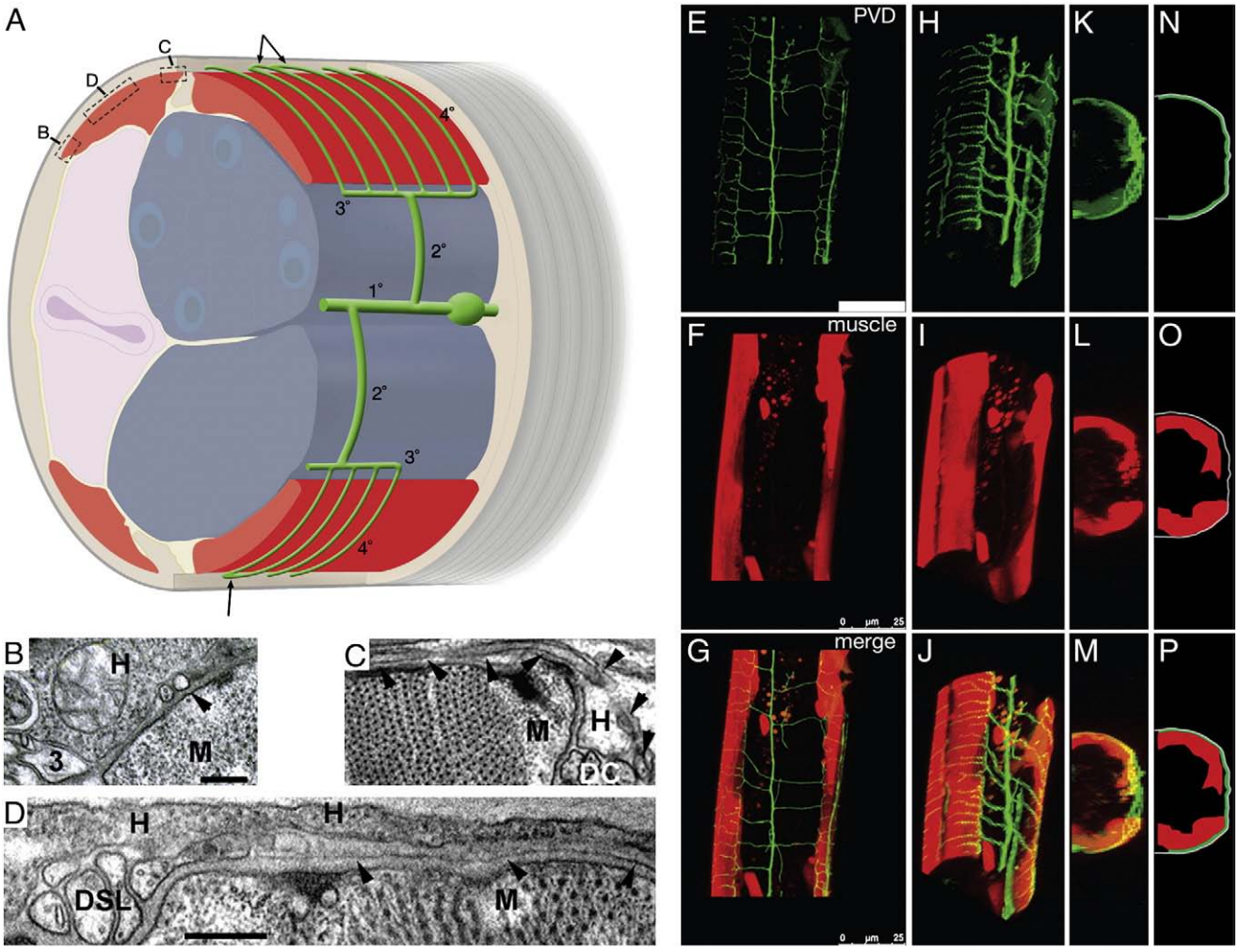

Fig. 2. PVD branches extend between muscle and the hypodermis. (A) Cartoon (oblique lateral view) shows the relative positions of the lateral PVD cell body and branches (green), the 1° process, two 2° processes, two 3° processes at the lateral margin of dorsal or ventral muscle quadrants (red), and many fine branches (4° processes) passing between the body-wall muscle (red) and the outer hypodermis (pale brown, most hypodermis has been cut away to view beneath it). Tiling of consecutive 4° branches while crossing the muscle quadrant is shown and occasional fusions of their terminal ends with neighboring 4° branches is indicated by arrows. Gonad, blue; Intestine, pale pink; Cuticle, grey. The relative length of 4° branches is exaggerated in this cartoon for the sake of clarity. Boxes indicate position of TEM images B, C, and D relative to muscle. (B) Transverse TEM image shows a presumptive 3° PVD branch (3), embedded in the lateral hypodermis (H) at the lateral edge of a dorsal body-wall muscle (M), and a much smaller presumptive 4° branch (arrowhead) seen in cross-section before moving beneath the muscle (animal N501C from the Hall archive). (C) Transverse TEM image of a PVD 4° branch (arrowheads) running laterally across the muscle, and then emerging medially, adjacent to the dorsal nerve cord (DC) (animal N2U, MRC archive). Note the much larger diameter of the dorsal cord axons, sublateral nerve axons, and 3° PVD process compared to PVD 4°. Scale bar indicates 200 nm for panels B, C. (D) Transverse TEM image of a PVD 4° branch (arrowheads) running laterally across the muscle quadrant near the dorsal sublateral nerve (DSL) (animal N501A from the Hall archive). Scale bar 200 nm. (E–P) 3-D reconstructions and projections of PVD in green (*F49H12.4*:GFP in E H, K, N), muscles in red (*myo-3*:dsRed2 in F, I, L, O) and merged images (G, J, M, P). Rotated confocal images (H–M) and schematic tracings (N–P) show PVD branches (green) extending over the body-wall muscle quadrants (red) and beneath the outer hypodermal layer (grey). Scale bar indicates 25 µm (E–G).

midline. Dorsal fine processes of FLP seem to fuse more extensively than do PVD fine processes.

Interestingly, electron microscopy suggests that 3° branches of PVD are positioned along the edge of the outer body-wall muscle quadrants and that branches emanating from PVDR and PVDL are positioned in a narrow space between the muscles and the outer hypodermis (Figs. 2B–D). Confirmation of this model is provided by confocal images of a transgenic strain expressing both *F49H12.4*:GFP (to mark PVD) and a muscle reporter (*myo-3*:dsRED2). Reconstruction of a Z-stack of confocal images clearly shows that PVD terminal branches (GFP) are closely apposed to the outside surface of each body-wall muscle quadrant (Figs. 2E–P).

Table 1

Genotype	Cells affected	Short name	Function of gene
Wild-type	None	N2	
mec-4(e1611)	Touch receptor neurons	—T	
ser-2prom3:DEG-3-N293I	PVD	—P	
ser-2prom3: DEG-3-N293I;*mec-4(e1611)*	PVD and touch receptor neurons	—TP	
mec-10p: DEG-3-N293I	PVD, FLP, and touch receptor neurons	—TPF	
mec-3(e1338)	PVD, FLP, and touch receptor neurons	*mec-3*	Transcription factor
mec-10(tm1552)	PVD, FLP, and touch receptor neurons	*mec-10*	DEG/ENaC subunit

Please cite this article as: Albeg, A., et al., *C. elegans* multi-dendritic sensory neurons: Morphology and function, Mol. Cell. Neurosci. (2010), doi:10.1016/j.mcn.2010.10.001

Genetic ablation of PVD and FLP neurons

For the purpose of exploring the behavioral roles of PVD and FLP, we generated transgenic lines in which these neurons are eliminated (Table 1). This was achieved using a constitutively active version of the nicotinic acetylcholine receptor (nAChR) channel subunit, *deg-3 (u662)*, which contains a I to N change at amino acid position 293 (or DEG-3-I293N) (Treinin et al., 1998). For selective ablation of PVD, we used the *ser-2prom3* promoter to drive selective expression in PVD and OLL neurons (Tsalik et al., 2003). In this transgenic line (*ser-2prom3*:DEG-3-N293I), PVD is specifically killed (−P). OLLs are unaffected by this transgene (supplemental Fig. 1), probably because the OLLs do not express DES-2, a nAChR subunit that is required for formation of functional DEG-3 receptors (Treinin et al., 1998). Combining the *ser-2prom3*:DEG-3-N293I transgene with the *mec-4 (e1611)* degeneration-causing mutation (Driscoll and Chalfie, 1991) led to the killing of PVD and the six touch receptor neurons (−TP). Last, expression of DEG-3-N293I from the *mec-10* promoter (*mec-10p:* DEG-3-N293I) led to the elimination of PVD, FLP, and the 6 touch receptor neurons (−TPF) (Huang and Chalfie, 1994). Analysis of these strains reproduced results of Way and Chalfie (1988), showing that PVD together with touch receptors are required for the avoidance response to high threshold mechanical stimuli (harsh touch) to the mid-body (supplemental Fig. 2). This result demonstrates the high penetrance of PVD and touch receptor degeneration in our strains as elimination of both PVD and touch receptors is required for the harsh touch response (Way and Chalfie, 1989). Moreover, elimination of the *mec-4* gene, and not of the touch receptors, does not eliminate high threshold mechanosensitivity of the touch receptor neurons (Suzuki et al., 2003).

PVD and FLP sensory neurons regulate C. elegans movement

Wild-type *C. elegans* placed on agar (solid surface) move via propagation of a sinusoidal-like waveform. Animals move constantly, mostly forward, namely head first. This movement is punctuated by short pauses and direction changes. These direction changes are achieved by short reversals, i.e. tail first (backwards) movement, or by sharp body bends — omega turns.

Visual observation of strains lacking PVD and FLP suggested that the elimination of these neurons altered overall movement. To quantify these defects, we recorded short movies of single animals from each PVD and FLP-ablated strain (−P, −TP, −TPF) and used custom designed image analysis software to compare them to video recordings from the wild-type control (N2) and from *mec-4(e1611)* (−T). This analysis confirmed that the overall movement of animals lacking PVD, FLP, and touch receptor neurons (−TPF) is significantly different from that of wild-type animals (Fig. 3). Specifically, −TPF animals are slower (Fig. 3A), pause more frequently (Fig. 3B), and make more reversals (Fig. 3C). Together these differences lead to increased dwelling (decreased displacement) of −TPF animals within a restricted area (Figs. 3D and E). These defects are unlikely to be a

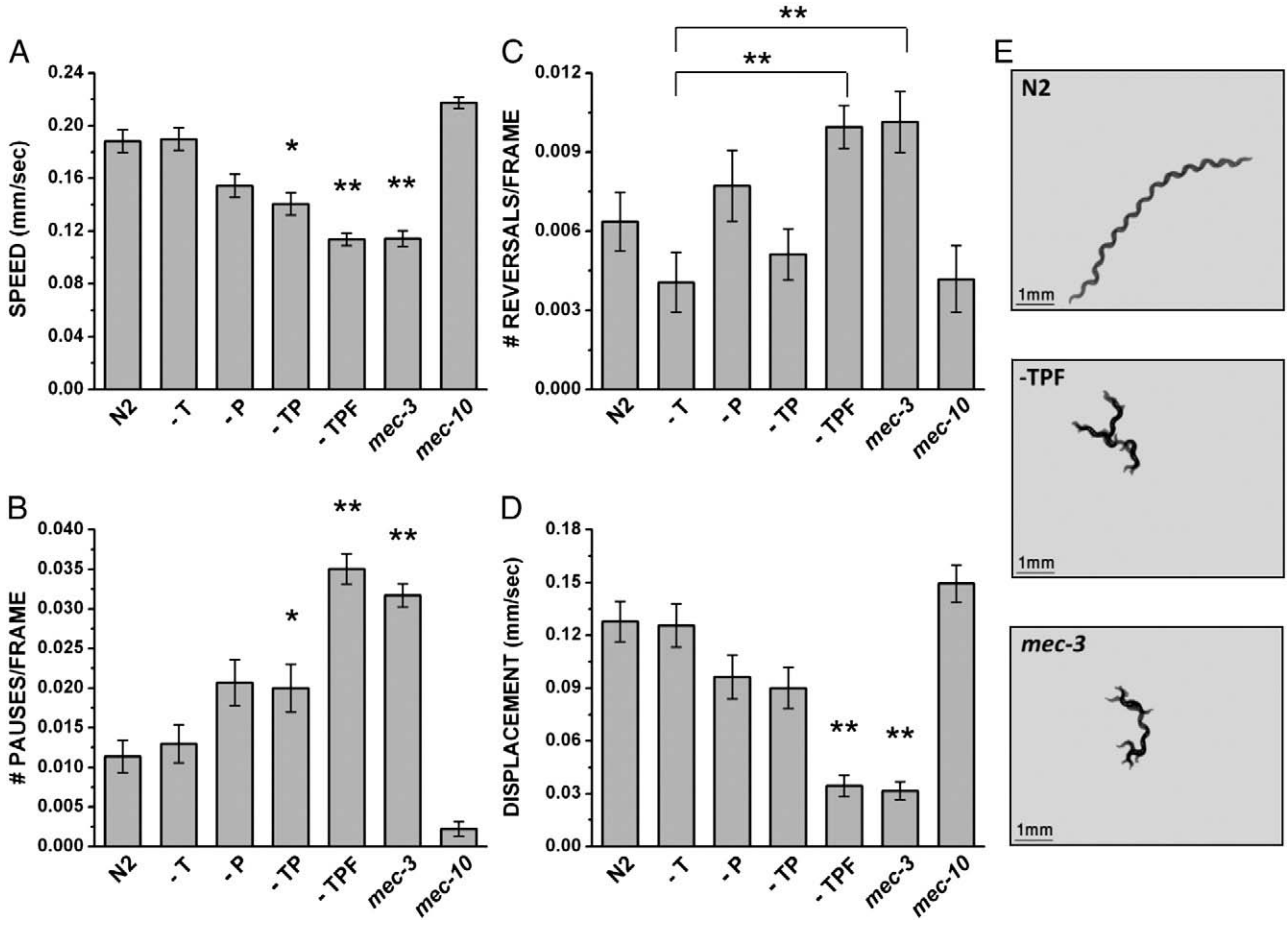

Fig. 3. Movement analysis in mutants defective for PVD and FLP. Movement was analyzed from movies of single adults from the following strains: N2 (n = 34), −T (n = 26), −P (n = 21), −TP (n = 24), −TPF (n = 30), *mec-3* (n = 19), and *mec-10* (n = 18). Significant differences relative to N2 (or relative to −T in C) are indicated by a single asterisk ($P<0.05$) or a double asterisk ($p<0.01$). (A) Speed (mm/s). Additional significant differences are: −T and *mec-10* relative to −TP, −TPF and *mec-3* ($p<0.01$) or to −P ($p<0.05$). (B) Number of pauses per frame. Additional significant differences are: −T and *mec-10* relative to −TPF and *mec-3* ($p<0.01$) (C) Number of reversals per frame. (D) Displacement in mm/s. Additional significant differences are: −T, −P and −TP relative to −TPF and *mec-3* ($p<0.01$) and for *mec-10* relative to −TPF and *mec-3* ($p<0.01$). (E) Representative tracings of a single animals' movement in one movie (superimposed pictures of all the frames of a movie). Movies are taken at a rate of 10 frames per second. Scale bar 1 mm.

Please cite this article as: Albeg, A., et al., *C. elegans* multi-dendritic sensory neurons: Morphology and function, Mol. Cell. Neurosci. (2010), doi:10.1016/j.mcn.2010.10.001

result of the lack of touch receptor neurons as −T animals are similar to wild-type in all of the parameters examined (Fig. 3). Effects on speed and number of pauses are likely to require elimination of both PVD and FLP, as animals lacking only PVD (−P and −TP) have an intermediate phenotype, between wild-type and −TPF: speed in mm/s of −P and −TP is 0.15 ± 0.008 and 0.14 ± 0.009 relative to 0.19 ± 0.008 and 0.11 ± 0.005 for wild-type and −TPF respectively, and number of pauses per frame of −P and −TP is 0.02 ± 0.003 and 0.02 ± 0.003 relative to 0.011 ± 0.002 and 0.035 ± 0.002 for wild-type and −TPF respectively (Fig. 3). Effects on the displacement and number of reversals, however, are likely to depend mostly on FLP, as strains having intact FLP (−P and −TP) are similar to wild-type. Although the PVD-lacking strains (−P and −TP) appear to show reduced displacement relative to wild-type, this difference is not significant and much smaller than the effect resulting from the combined elimination of PVD, touch neurons and FLP (−TPF) (Fig. 3D). Together, the defects seen in animals lacking PVD and FLP lead to increased dwelling within a restricted area and suggest that PVD and FLP function to promote an escape response, as is seen in the harsh touch response. These results also suggest that PVD and FLP are active under normal growth conditions and in the absence of acute stimuli.

Genetic analysis has established that the *mec-3* transcription factor is required for the mechanosensitive function of PVD and FLP (Way and Chalfie, 1988). *mec-3* animals show overall sluggish movement that resembles that of animals lacking PVD and FLP. This similarity is strikingly confirmed by movement analysis, showing near identity between movement defects of −TPF and *mec-3* animals (Fig. 3). It is interesting to note that *mec-3* is required for the elaboration of the PVD dendritic arbor; in *mec-3* mutants the PVD neurons display lateral primary (1°) dendritic processes projecting along the each side of the animal but not the side branches (2°, 3°, and 4° (Tsalik et al., 2003)). Thus, the movement defect of *mec*-3 and −TPF mutant animals is correlated with the absence of the PVD sensory network. *mec*-3 is also required, however, for expression of the MEC-10 DEG/ENAC ion channel (Huang and Chalfie, 1994) which was recently shown to mediate the response of PVD to high threshold mechanical stimuli (Chatzigeorgiou et al., 2010). Interestingly, our analysis of *mec-10(tm1552)* animals does not show movement defects resembling those of either *mec-3* or −TPF mutant animals (effects of *mec-10* on speed and the number of pauses are opposite to those of −TPF and *mec-3* animals, Figs. 3A and B). Thus, defective *mec-10*-dependent mechanosensation does not account for the movement defects shown in *mec-3* mutants. MEC-3, however, is required for expression of many additional genes (Zhang et al., 2002) in the touch neurons and could therefore drive expression of other functional components that are necessary for the normal roles of PVD and FLP in locomotion.

PVD is required for maintaining normal body posture and responds to body-bending

Our analysis of PVD morphology shows that PVD terminal (4°) branches grow across the muscle quadrants (Fig. 2). The position of these branches in close contact with the contractile apparatus seems well-suited to a potential role as a proprioceptor monitoring muscle tension. If PVD neurons function as proprioceptors, their elimination should lead to postural defects, i.e., to changes in the waveform (shape) of animals lacking these neurons.

To examine this possibility we quantified several parameters that characterize the nematode's waveform. These metrics, described in Fig. 4A, were chosen as they do not depend on the assumption that animals adopt regular sinusoidal movement. They are based on drawing a skeleton (central line) along the animal's body, and a straight line connecting the nose to the tail. The number of points where the two lines intersect is the cut-point number. The amplitude corresponds to the vertical distance from the straight line to the skeleton. Amplitude was normalized to body length (supplemental Fig. 3) in order to eliminate effects of differences in body length on amplitude. The body-bending angle was measured between adjacent short segments on the skeleton (for details see methods).

Careful analysis of animals lacking PVD neurons (−P) detected differences in their waveform, specifically, −P animals show reduced bending angle and cut-point number, but no change in the average amplitude of the waveform (Fig. 4). These results suggest a longer wavelength in animals lacking PVD. Indeed, the measured wavelength of −P animals is 0.578 ± 0.005, relative to 0.559 ± 0.008 for N2 animals. However, this difference is not significant. Note that irregularities in the speed and direction of wave propagation make the extraction of the animals' wavelength difficult, as demonstrated in supplemental Fig. 4. Differences in bending angle and cut-point number are unlikely to be a result of the smaller length of −P animals relative to wild-type, as other strains used in this analysis (−P, −T, −TP, −TPF, and *mec-3*) are similarly short (supplemental Fig. 3) but show large differences in bending angle and cut-point number (supplemental Fig. 5).

To examine the full distribution of the postural parameters across a population of animals from the same strain, we used graphs of the cumulative distribution function of each parameter. This gives a graphical representation of the variability. Interestingly, this analysis showed that the differences in the averages reflect a shift of the whole distribution in mutant animals relative to wild-type animals, but the *shape* of the distribution stays essentially the same (Supplemental Fig. 6). Thus these mutants are still capable of regulating posture via other sensory mechanisms.

TEM analysis described above suggests that FLP terminal branches, like PVD terminal branches (4°), contact the outer surface of head muscles and therefore could function as proprioceptors in this body region. Indeed, we find strong defects in posture of −TPF and *mec-3 (e1338)*. Both −TPF and *mec-3* animals have different waveform amplitude relative to −P and wild-type animals, and thus appear to have distinct and significant effects on the waveform of animals (supplemental Fig. 5). Since the bending angle, amplitude, and cut-point number of −TPF animals are significantly different from those of −T animals ($p<0.01$; supplemental Fig. 5), differences in posture between −P and −TPF are unlikely to result from the lack of touch cells in −TPF. Rather, we suggest that FLP, like PVD, is likely to be required for regulating posture. Interestingly, and as noted by Li et al. (2006), the bending angle in *mec-3* animals is similar to wild-type, and thus unlike the bending angle of animals lacking PVD and/or FLP. However, in *mec-3* animals the two other indicators for body posture, amplitude and cut-point number, are significantly different relative to wild-type animals, and are similar to what is seen in −TPF animals. Thus, we suggest that side branches of PVD and FLP whose outgrowth requires MEC-3 (Tsalik et al., 2003) are important for sensing muscle tension and thus for waveform regulation. *mec-10* animals are similar to −P in having similar average angle as −P, but their cut-point number is intermediate between N2 and −P (Fig. 4). Overall, our results show distinct defects in the strains examined, indicating that while each of MEC-10, MEC-3, PVD, or FLP has a role in regulating posture, none of them alone can fully explain the waveform defects seen in animals lacking PVD and FLP.

The results described above suggest a role for PVD in sensing and controlling body posture. Such a role requires that PVD will be sensitive to movement-dependent changes in muscle tension. To examine whether PVD respond to movement, we expressed YC2.3, a reporter for calcium levels, in PVD using an *egl-46* promoter. Using this reporter we could image activation of PVD by strong temperature downshifts or high threshold mechanical stimulation (Chatzigeorgiou et al., 2010). To examine the response of PVD to movement we used the same approach used by Li et al. (2006) for analysis of DVA, also shown to function as a proprioceptor. This approach consists of imaging animals that are glued around the tail to immobilize the PVD cell body (Fig. 5A) but are otherwise allowed to freely move the rest of

Please cite this article as: Albeg, A., et al., *C. elegans* multi-dendritic sensory neurons: Morphology and function, Mol. Cell. Neurosci. (2010), doi:10.1016/j.mcn.2010.10.001

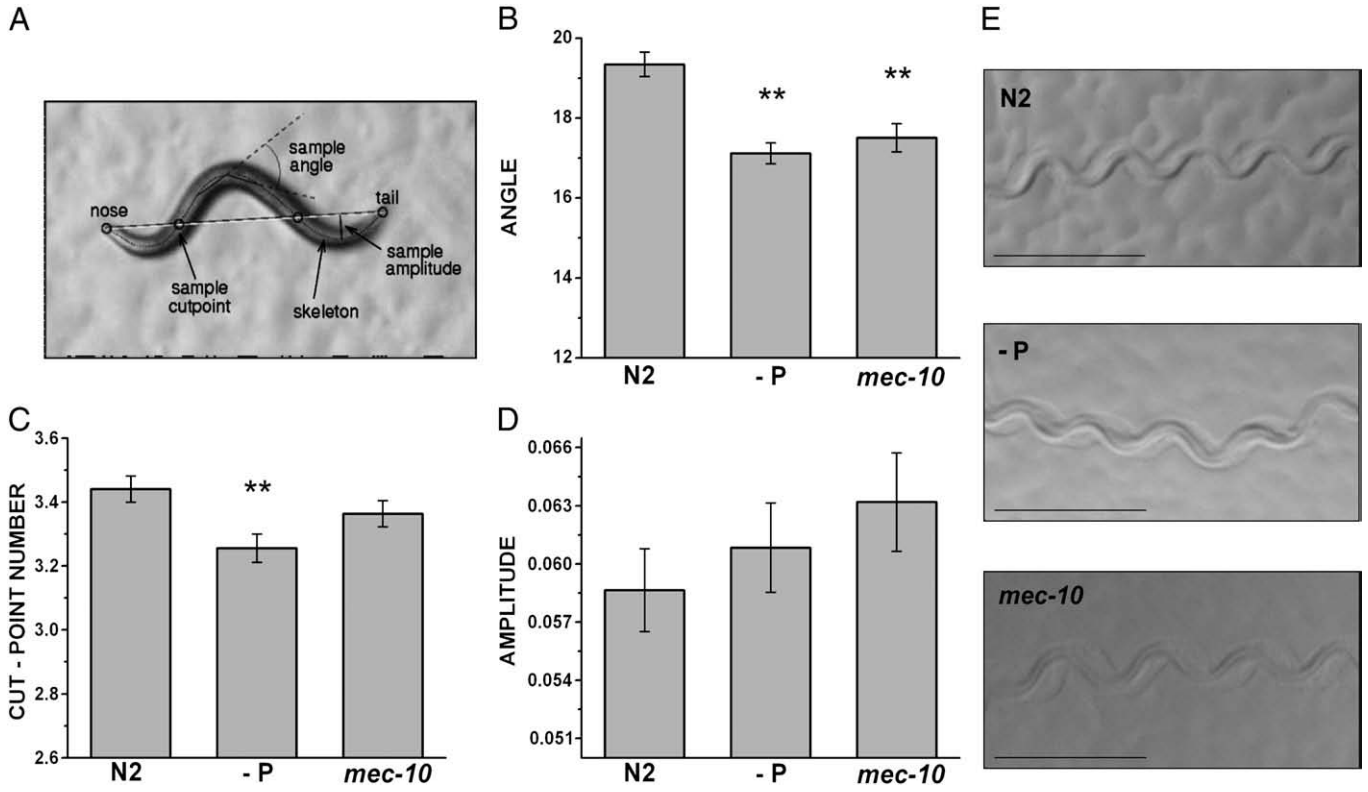

Fig. 4. Postural defects in animals lacking PVD. Analysis of N2 (n = 34), −P (n = 21), and *mec-10* (n = 18). Significant differences relative to N2 are indicated by a double asterisk ($P<0.01$). (A) Diagrammatic representation of parameters used for postural analysis. Circles surround cut-points between the central body axis or "skeleton" and a straight line connecting the head and tail. (B) Average bending angle. (C) Cut-point number. (D) Average amplitude. For each animal the amplitude is divided by the length in mm. (E) Representative tracks of animals from the different strains. Scale bar 1 mm.

their body in saline. In these animals clear calcium transients are observed (n = 26; Figs. 5B–E, H). As a control we immobilized animals completely by gluing along the body of the worm. Under these conditions the worms show very little movement and no calcium transients were measured in PVD, although a gradual decline in the YFP/CFP ratio is seen likely to be a result of bleaching (n = 11; Figs. 5F,

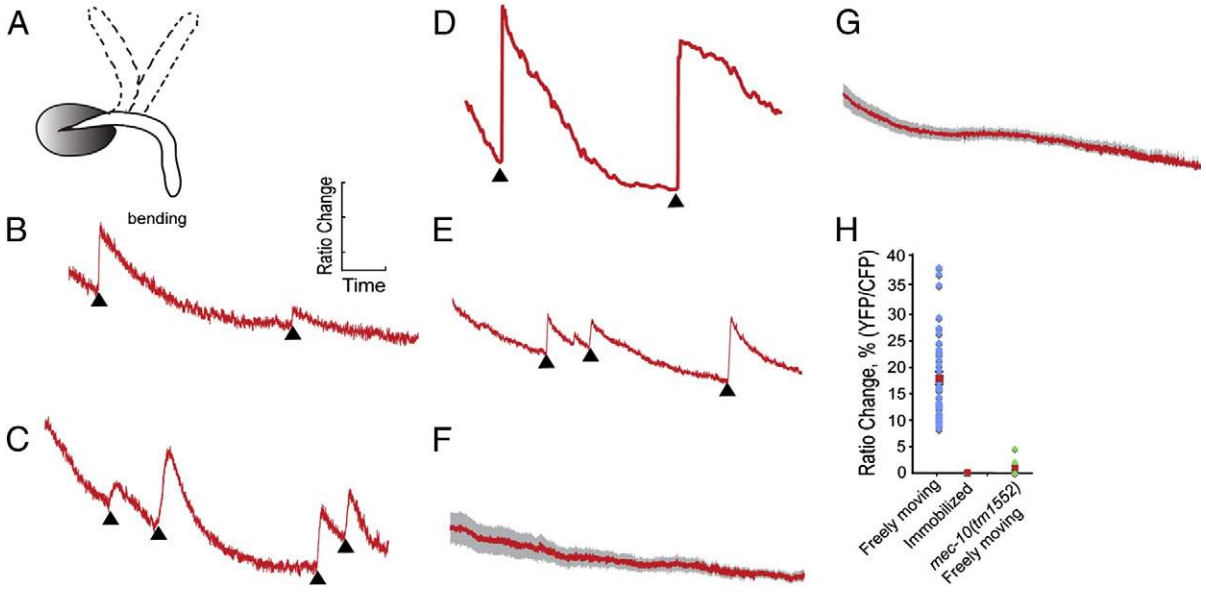

Fig. 5. Calcium imaging of PVD during movement. (A) A worm with its tail glued to the substrate as shown in the schematic is able to bend anterior regions of the body. (B–E) Body-bending evokes Ca^{2+} transients in PVD. Shown are sample traces from different wild-type worms. The red trace represents the percentage change in the YFP/CFP ratio, R/R_0. The scale bar represents a ratio change of 20% and a time interval of 20 s. Black arrows indicate the onset of a series of bending movements. (F) Worms glued along the length of the body were unable to bend and no Ca^{2+} transients were detected. The red trace represents the average R/R_0 and grey shading indicates SEM. This trace represents the average of 11 animals. (G) *mec-10(lf)* animals glued at the tail. The red trace represents the average R/R_0 and grey shading indicates SEM. This trace represents the average of 10 animals. (H) Scatter plot of R/R_0 for fully restrained and partially restrained animals (R_0 is the lowest point at the start of a transient and R is the peak value, a value of zero was assigned to traces having no transients). In traces where several transients were shown we calculated the average of all transients. The mean is shown as a red square. Error bars indicate SEM. Also shown are individual data points for each condition (26 partly restrained wild-type (40 transients analyzed), 11 immobilized wild-type, and 10 partly restrained *mec10 (tm1552)* animals). (For interpretation of the references to color in this figure legend, the reader is referred to the web version of this article.)

Please cite this article as: Albeg, A., et al., *C. elegans* multi-dendritic sensory neurons: Morphology and function, Mol. Cell. Neurosci. (2010), doi:10.1016/j.mcn.2010.10.001

H). Importantly, appearance of calcium transients in partly immobilized animals correlates with initiation of body bends supporting our hypothesis that PVD responds to body posture (Figs. 5B–E).

MEC-10 was shown to function in PVD mechanosensation (Chatzigeorgiou et al., 2010) and *mec-10* mutants display postural features resembling that of −P animals (Fig. 4). Thus MEC-10 dependent mechanosensitivity of PVD may be required for its response to posture. To examine this possibility we looked for posture dependent calcium transients in *mec-10* animals. This analysis shows no calcium transients in mutant PVD (n = 10, Fig. 5 G, H). Thus MEC-10 is likely to function as the mechano-transduction channel enabling the response of PVD to posture.

Noxious mechanical stimulation inhibits egg-laying via PVD and FLP

PVD neurons are born at the second larval stage (L2), their primary (1°) longitudinal branches extend during L3, and their full branching pattern is only seen towards the end of the fourth larval stage (Oren-Suissa et al., 2010; Smith et al., 2010). FLP neurons are generated in the embryo but do not produce side branches until after hatching; anti-DEG-3 staining shows simple unbranched FLP processes until the late L3 when both PVD and FLP begin to elaborate side branches from their fully extended longitudinally arrayed primary dendritic processes. The final FLP branching pattern, like the mature PVD dendritic arbor, is not fully established until the end of L4 (Fig. 6). Thus, the elaboration of the FLP dendritic network is apparently delayed for a period during late embryogenesis and early larval development and then is finally initiated in coordination with the emergence of side branches for PVD.

The late appearance of PVD and FLP side branches (2°, 3° and 4°) suggests that they may be required for adult functions. One important adult function is egg-laying. Mechanical stimuli via the touch receptor neurons were previously shown to inhibit egg-laying (Sawin, 1996), and gentle touch applied to the posterior body led to increased intervals between calcium transients, in HSN neurons regulating egg-laying (Zhang et al., 2008). Thus low threshold mechanical stimulation via the touch receptor neurons leads to a decrease in egg-laying. Nothing, however, is known about the effects of high threshold mechanical stimulation on egg-laying. To examine the effects of high threshold mechanical stimulation we measured egg-laying rates following a particularly stressful mechanical stimulus, i.e. transfer with a wire pick to a new plate. This manipulation was shown to promote an escape response and to require MEC-3, suggesting that it is a response to mechanical stimulation (Zhao et al., 2003). Initially, we determined the normal egg-laying rate for each strain. This analysis was done by counting eggs laid two hours following transfer of single animals to a fresh plate. This approach assumes that effects of transfer are transient and indeed the egg-laying rate of N2 obtained this way (4.15 ± 1.13 (n = 13) and supplemental Fig. 7) is similar to the egg-laying rate obtained using an automated tracking system (3.5 ± 0.5 (n = 40), (Waggoner et al., 1998)). We used these results to calculate the average egg-laying rate per half hour and compared these values to the rate of egg-laying during the first half hour following transfer. Results of this analysis show strong inhibition of egg-laying in the first half hour after transfer (strong mechanical stimulation); only 23% of wild-type (N2) animals laid eggs during the first half hour and their egg-laying rate was reduced relative to the expected rate for the same strain (Fig. 7). This inhibition is eliminated in −TPF animals (62% of animals lay eggs in the first half hour and the egg-laying rate is significantly higher $p<0.01$, Fig. 7). In −T animals lacking only touch receptor neurons 50% of animals lay eggs in the first half hour but egg-laying rate is only slightly higher than in wild-type and is significantly lower relative to −TPF animals ($p<0.01$, Fig. 7). Thus touch receptor neuron mediated inhibition of egg-laying is either too transient or too small to be detected in our assay. Animals lacking only PVD (−P) have an intermediate phenotype (56% of animals laid eggs and egg-laying rate was in between wild-type and −TPF, Fig. 7), suggesting that PVD and FLP are required together for

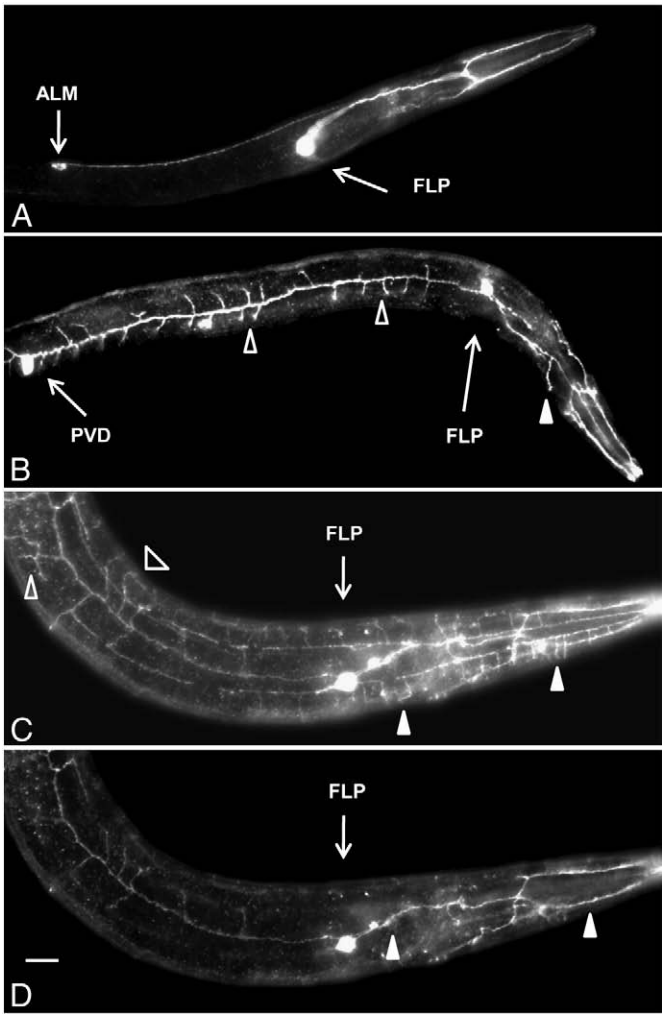

Fig. 6. FLP side branches appear late in development. Z-stacked images of DEG-3 staining from synchronized N2 animals. (A) Second larval stage, PVD is not seen. Indicated is the ALM neuron. (B) Third larval stage. Indicated are representative 2° branches belonging to PVD (empty arrow heads) and FLP (filled arrow head). (C) Late fourth larval stage. Indicated are representative 4° branches belonging to PVD (Empty arrow head) and FLP (Filled arrow head). (D) Single section from the same animal as in C, showing only the major FLP branches (filled arrow heads). Scale bar 0.01/mm for A–D.

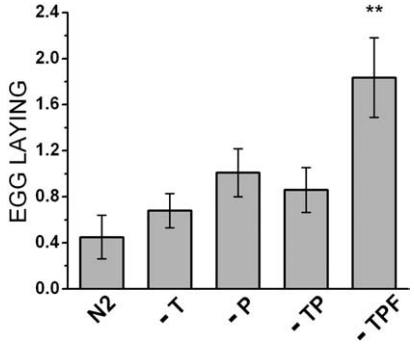

Fig. 7. Inhibition of egg-laying by noxious mechanical stimuli. Number of eggs laid in the first half hour following transfer with a wire pick divided by average number of eggs laid by the same strain per half an hour, in N2, −T, −P, −TP, and −TPF, n = 29–33 each. Significant differences relative to N2 are indicated by a double asterisk ($P<0.01$). −TPF is also different from −T, ($p<0.01$).

Please cite this article as: Albeg, A., et al., *C. elegans* multi-dendritic sensory neurons: Morphology and function, Mol. Cell. Neurosci. (2010), doi:10.1016/j.mcn.2010.10.001

effects on both the fraction of animals laying eggs and on the egg-laying rate.

Discussion

PVD and FLP are highly branched neurons that envelop the entire adult animal with an elaborate network of sensory processes. These neurons occupy four distinct non-overlapping sensory fields: left side of the body, right side of the body, left side of the head, and right side of the head. PVD and FLP are similar in being multi-dendritic and in expression of the MEC-3 transcription factor, a key regulator of fate in *C. elegans* mechanosensors (Way and Chalfie, 1988, 1989). This similarity, together with lack of overlap between sensory fields of PVD and FLP, suggests that they perceive the same sensory stimuli. Accuracy and efficiency of the response to specific sensory stimuli requires accurate tiling of sensory fields. Indeed, processes of PVD and FLP do not overlap and this tiling is likely to be an active process requiring retraction of overlapping processes (Smith et al., 2010). Both PVD and FLP arborize to produce candelabra-like structures. The multi-dendritic morphology of PVD and FLP and the position of their sensory processes below the outer envelope of the animal are similar to the morphology and subdermal location of mammalian and *Drosophila* nociceptors (Tracey et al., 2003). Indeed, PVD neurons were shown to function in the response to harsh touch and to cold temperatures suggesting that they function as nociceptors (Way and Chalfie, 1989; Chatzigeorgiou et al., 2010).

Our analysis shows that animals lacking PVD and FLP neurons have reduced speed, increased number of pauses, and an increase in the number of reversals. Thus animals lacking PVD and FLP tend to dwell more within a restricted area. This phenotype of animals lacking PVD and FLP is seen under normal growth conditions and in the absence of acute stimuli suggesting that under such conditions PVD and FLP function to promote increased speed, reduced number of pauses, and reduced number of reversals, and thus to suppress dwelling. Since *mec-10* animals do not demonstrate similar defects, mechanical stimulation sensed by MEC-10 is unlikely to be responsible for these effects on movement. Thus the nature of the stimuli activating PVD and FLP under the conditions used in this study is not known. Neither can we conclude that this stimulus/stimuli is/are noxious. However, the similarity between the suggested effects of PVD and FLP on movement and the effects of harsh touch and transfer by a platinum wire on movement (Way and Chalfie, 1988; Zhao et al., 2003), suggest that these effects represent an escape response from noxious signals. While the conditions used in our experiments are not known to be noxious, low-level noxious signals present in these conditions may be sufficient to suppress dwelling. Alternatively, signaling pathways mediating noxious signals in PVD and FLP may have low constitutive activity sufficient for the dwelling suppression that we observe. We note that stimulation of PVD by cold leads to increased omega turns, a behavior that like reversals promotes dwelling within a restricted area (Chatzigeorgiou et al., 2010). Thus effects of cold on behavior appear to be opposite to the effects of harsh touch and are in contradiction to our hypothesis that stimulation of PVD and FLP promotes an escape response and inhibits dwelling. One possible explanation for this disparity is that distinct stimuli activate different groups of neurons leading to unique behavioral responses. For example, these results are consistent with the suggestion that activation of both PVD and FLP by transfer with a wire pick leads to an escape response whereas activation of PVD alone by cold leads to omega turns. Other explanations such as differences in the experimental conditions—specifically the cold response was assayed in liquid and not on agar plates—may also explain this discrepancy.

The escape response is an important behavioral reaction to noxious stimuli. Activation of sensory neurons in the tip of the head is likely to result in reversals or turns, leading to avoidance of the noxious signal. However, the best strategy for escape from noxious stimuli perceived by sensory endings in the body is likely to involve the alternative strategy of inhibiting reversals and increasing the overall rate of locomotion. This idea is supported by the finding that mechanical stimulation mediated by both low and high threshold receptors results in the inhibition of reversals (Zhao et al., 2003). In addition, noxious signals that trigger an escape response are also likely to inhibit behaviors that might endanger the next generation, such as egg-laying. The reduced inhibition of egg-laying by high threshold mechanical stimuli in animals lacking PVD and FLP suggests that these neurons normally evoke both the escape response and inhibit egg-laying in animals exposed to noxious stimuli. Here we note that PVD and touch receptor neurons are redundant in mediating the harsh touch dependent escape response (Way and Chalfie, 1989; Chatzigeorgiou et al., 2010). Thus our results suggesting a role for PVD and FLP in harsh touch dependent inhibition of egg-laying provides these neurons with a previously unknown role, a role that is not redundant with the roles of the touch receptor neurons.

The arborization pattern of PVD and FLP produces a large number of closely spaced terminal branches (4° branches); for PVD we show that these terminal branches grow across the body-wall muscle quadrants. Thus muscle tension is likely to be sensed by these terminal branches. Indeed, animals lacking PVD are defective for posture and calcium transients are observed in PVD in response to movement. Animals lacking PVD and FLP show distinct postural defects relative to animals lacking only PVD. These results support the idea that terminal branches of both PVD and FLP function as proprioceptors, providing a feedback loop enabling control of muscle tension. In addition, our results show that animals lacking PVD maintain an altered but regular waveform. Thus PVD is likely to act redundantly with other body proprioceptors. Indeed, DVA and the sensory branches of motor neurons have also been suggested to function as proprioceptors (Li et al., 2006; Tavernarakis et al., 1997).

In mammals proprioceptors are part of local feedback loops responsible for regulating tension of specific muscles. The sensory fields of PVD and FLP, however, include multiple muscles and thus are unlikely to function within such local circuits. Instead, they may function in more global control of body-wall muscles' (PVD) or head muscles' (FLP) tension. In *Drosophila,* proprioceptors were suggested to function in enabling efficient propagation of muscle contractions needed for movement of larva (Hughes and Thomas, 2007). This study suggested a mechanism whereby local feedback loops enable efficient propagation of muscle contractions. Similarly, movement phenotypes in animals lacking PVD and FLP may be a byproduct of the postural defects in animals lacking these cells. However, current knowledge of PVD and FLP connectivity does not support local feedback loops as a mechanisms linking these two phenotypes (White et al., 1986). Nonetheless, we cannot rule out a causal relationship between the two phenotypes.

PVD neurons first appear during the second larval stage and their mature branching pattern is only seen in adults. FLP neurons are born earlier, in the embryo, but the emergence of FLP side branches is apparently delayed until larval development and coincides with the elaboration of the PVD dendritic arbor. This developmental pattern suggests that the elaborate branching patterns of these neurons may not be required until late in development. Two non-exclusive explanations for this finding are: 1) A dense network of sensory processes is only required in adults due to their larger circumference; 2) Sensory endings of PVD and FLP are required for perceiving sensory stimuli regulating adult specific behaviors. Our results showing that PVD and FLP regulate egg-laying (an adult specific behavior) support the second suggestion. We note that neither PVD or FLP are known to synapse into the egg-laying circuit (White et al., 1986), thus the effects of PVD and FLP on egg-laying may require non-synaptic signaling by diffusible signals such as neuropeptides. Thus, our results suggest that an important function of PVD and FLP is to regulate egg-laying. Egg-laying, however, is not the only behavior regulated by

Please cite this article as: Albeg, A., et al., *C. elegans* multi-dendritic sensory neurons: Morphology and function, Mol. Cell. Neurosci. (2010), doi:10.1016/j.mcn.2010.10.001

these cells. Movement and posture, both regulated by PVD and FLP, are not adult specific behaviors. Moreover, FLP are born during embryogenesis and are known to function in avoidance of mechanical stimuli to the head (Kaplan and Horvitz, 1993), this function may not require FLP side branches that appear late in development. Unfortunately, data on larval roles of PVD, FLP or other *C. elegans* neurons is scarce.

In mammals, the somatosensory system is responsible for multiple functions, a result of multiple types of sensory neurons having different morphological and functional properties. Similarly in *Drosophila* DA sensory neurons are a heterogeneous group of neurons enabling multiple functions. For example noxious signals are perceived by multi-dendritic neurons whereas muscle tension is sensed by poorly branched proprioceptors (Hughes and Thomas, 2007). Our work suggests that FLP and PVD function as both nociceptors and proprioceptors. The ability of these *C. elegans* neurons to perform multiple functions is a simple solution for enabling a complex behavioral repertoire in an animal having such a small assortment of neurons.

Experimental methods

Imaging of PVD and FLP morphology

Anti-DEG-3 antibodies and DEG-3 staining methods were utilized as previously described (Yassin et al., 2001). The *F49H12.4*:GFP reporter for visualizing PVD was previously described (Watson et al., 2008). A *mec-7:*RFP reporter was utilized to visualize FLP morphology (Hamelin et al., 1992). The body-wall muscle marker was *myo-3: dsRed2* (Fire and Waterston, 1989). TEM analysis was undertaken principally on serial section images of the archival animal "N2U" provided from the MRC collection of John White and Jonathan Hodgkin. Additional studies were done on other wild-type adult animals in the Hall archives. Many serial images of animal N2U can also be viewed on the website www.wormimage.org. Click on the N2U "color code" to see some of the codes assigned to fine branches of FLP and PVD by Eileen Southgate and John White.

Generation of transgenic strains PVD and FLP

To enable killing of neurons we used a 3.2 kb genomic fragment starting from the *deg-3* ATG, containing the entire *deg-3(u662)* (DEG-3-N293I) coding region and 3′ untranslated region sequences (Treinin and Chalfie, 1995). This fragment was inserted downstream of a 4.1 kb *ser-2prom3* promoter fragment (Tsalik et al., 2003), or a 2.4 kb *mec-10* promoter fragment (Huang and Chalfie, 1994). These constructs were injected at 5 ng/μl together with *dpy-20* DNA (20 ng/μl), and SKII^{-} (100 ng/μl) to *dpy-20(e1282)* animals. Transgenes were integrated into the genome using UV (Mitani, 1995) and out-crossed before analysis.

Movement and posture analysis

Animals for movement and posture analysis were picked as L4 to fresh plates and grown overnight to adulthood at 20 °C. For image analysis single adults were picked to a fresh NGM plate (pre-equilibrated at 20 °C) having a thin layer of OP50 (overnight growth) and allowed to acclimate for 10 min at 20 °C. Movement of each animal was then recorded at a 25× magnification and at a rate of 10 frames per second. Animals were recorded for 60 s or until they moved out of the frame. These movies were analyzed using software developed for this purpose (detailed description of this software is provided in http://www.cs.huji.ac.il/~feit/worms/user-manual.pdf).

In brief, the animal was identified using a threshold on grey levels and then a skeleton (central line) was generated for each frame. The head was identified automatically and checked for consistency across frames; this was then verified manually. Movement in each frame was identified as *forward* (movement of the skeleton's midpoint towards the position of the head in the previous frame), *backward* (reversal, movement of the midpoint away from the position of the head in the previous frame), *pause* (midpoint movement of less than 0.05 mm/s), or *omega turn* (when a straight line connecting the head and tail does not intersect with the skeleton except at the ends and the maximal amplitude is >40% of the skeleton length). Consecutive frames having the same type of movement form a single segment. Thus, we could quantify the number of segments of each type of movement, the time spent in different types of movement, and attributes of movement such as speed and posture for each type of movement.

Speed is an average in mm/s for all frames of forward or backward movement. Displacement is the net distance in mm traversed by the animal's centroid in the first 15 s of the movie. Only a few animals escaped the frame within less than 15 s; in these cases the displacement used is the distance traversed by the centroid between the first and last frame analyzed. Therefore, the net displacement was normalized by dividing by the duration (in seconds) of the analyzed segment. This measurement integrates information on speed, percentage of time spent in pauses, and rate of reversals, as each of these factors affects the average net displacement per second.

Cut point number is the number of times the worms' skeleton intersects with a straight line connecting the animal's nose to its tail, including the end points. As pixels are discrete, "intersection" means a distance from the skeleton of less than a pixel. A sequence of 3 or more skeleton points at a distance of more than 1.4 pixels (the diagonal of a pixel, needed to account for possible variations in orientation) is required between successive cut-points.

Average bending angle is a measure of the curvature along the worm. Angles are measured from the head towards the tail, and are in the range of $\pm 180°$, indicating an inclination to the left (positive) or to the right (negative). Angles are measured as follows. Consider three skeleton points *a*, *b*, and *c*. The angle at point *b* is the angle between the continuation of the line from *a* to *b* and the line from *b* to *c*. Thus if the worm is completely straight, the angle will be 0. The distances from *a* to *b* and from *b* to *c* are one twelfth of the skeleton length (see Fig. 4A for a diagrammatic representation). The average bending angle is the average of the absolute values of the angle as measured for *all* skeleton points, except within one twelfth of the length from the ends. Avoiding the ends reduces the effect of foraging behavior. Due to using the absolute values, positive and negative angles (inclination to left or right) do *not* cancel out.

Average amplitude is the average distance in pixels from each point in the skeleton to the line connecting the nose and the tail. Postural parameters (bending angle, cut-point number, and average amplitude) are taken from segments of forward movement. To eliminate differences in amplitude that are a result of skeleton length, the average amplitude was divided by the skeleton length (mm) to produce a normalized average amplitude.

Wavelength is ill-defined for many of the frames, as the worm shape does not resemble a sinusoidal posture (see supplemental Fig. 4). We therefore use the following procedure to both identify frames where the posture is wave-like and find the wavelength. First, we smooth the angles by averaging over a window of 3 in either direction. Then we find the minimal and maximal signed angle on either side of the worm's midpoint. The wavelength is the distance between the skeleton points with the two maximal angles, or the points with the two minimal angles, subject to the requirement that maximal or minimal angles used also have an absolute value of more than 13°. Otherwise, the wavelength is not defined for this frame. If both maxima and both minima have an absolute value of more than 13°, the pair where the smaller absolute value is larger is selected. Note that with this definition the wavelength is the straight distance between two extremum points, similar to the conventional physical definition of wavelength, but different from the definition used by

Please cite this article as: Albeg, A., et al., *C. elegans* multi-dendritic sensory neurons: Morphology and function, Mol. Cell. Neurosci. (2010), doi:10.1016/j.mcn.2010.10.001

Korta et al. (2007) who measured the length along the worm's skeleton. The normalized wavelength is the wavelength divided by the skeleton length.

For (normalized) average amplitude and angle the average is first calculated for all the skeleton points in each frame of forward movement. Then the median of these averages is found using all such frames in each movie. Finally, the value reported in Fig. 4 is the average for all movies from the same strain. Numbers are average ± standard error of means. Statistical analysis was done using Anova with the Bonferoni correction using Origin 7.O data analysis package.

Calcium imaging

Optical recordings of PVD performed as described (Chatzigeorgiou et al., 2010) on a Zeiss Axioskop 2 upright compound microscope equipped with a Dual View beam splitter and a Uniblitz Shutter. Fluorescence images were acquired using MetaVue 6.2. Filter-dichroic pairs were excitation, 400–440; excitation dichroic 455; CFP emission, 465–495; emission dichroic 505; YFP emission, 520–550. Individual adult worms (~24 h past L4) were glued over the entire length of their body or partially glued around the tail region with Nexaband S/C cyanoacrylate glue to pads composed of 2% agarose in extracellular saline (145 mM NaCl, 5 mM KCl, 1 mM $CaCl_2$, 5 mM $MgCl_2$, 20 mM D-glucose, 10 mM HEPES buffer, pH 7.2). Worms were allowed to freely bend in the saline. Acquisitions were taken at 10 Hz (100 ms exposure time) with 4×4 binning, using a 63× Zeiss Achroplan water immersion objective. Approximately 3000 frames were captured. Calcium peaks were analyzed using custom made software. The ratio change percentage was calculated as R/R_0 as described in (Kerr et al., 2000).

Egg-laying assays

For egg-laying assays L4 animals were picked to fresh plates for overnight growth to adulthood. For experiments, individual adults were picked to fresh plates using a wire pick and the number of eggs laid was counted half an hour and 2 h following transfer. The expected number of eggs laid over half an hour period is obtained by dividing the average number of eggs laid by a specific strain over a 2-hour period by 4.

Acknowledgments

This research was supported by U. S.–Israel Binational Science Foundation Grant 2005036 (MT and DMM), by NIH R21 NS6882 and R01 NS26115 (DMM), and by NIH RR12596 (to DHH). We thank John White and Jonathan Hodgkin for the donation of the MRC/LMB electron microscopy archives to the Hall lab, the *C. elegans* Genetic Center for strains, Hezi Gottlieb for help with image acquisition, Gady Brinker for help with image analysis software, Chris Crocker for the artwork in Fig. 2, Dattananda Chelur for the *mec-10* promoter, Sylvia Lee for the *mec-7:RFP* transgenic line, and Jessica Von Stetina for generating *myo-3:dsRed2* animals.

Appendix A. Supplementary data

Supplementary data to this article can be found online at doi:10.1016/j.mcn.2010.10.001.

References

Caterina, M.J., Julius, D., 1999. Sense and specificity: a molecular identity for nociceptors. Curr. Opin. Neurobiol. 9, 525–530.
Chalfie, M., Sulston, J., 1981. Developmental genetics of the mechanosensory neurons of *Caenorhabditis elegans*. Dev. Biol. 82, 358–370.
Chatzigeorgiou, M., Yoo, S., Watson, J.D., Lee, W.-H., Spencer, W.C., Kindt, K.S., Hwa, S.W., Miller III, D.M. I., Treinin, M., Driscoll, M., Schafer, W.R., 2010. Specific roles for DEG/ENaC and TRP channels in touch and thermosensation in C. elegans nociceptors. Nat. Neurosci. 13, 861–868.
Driscoll, M., Chalfie, M., 1991. The *mec-4* gene is a member of a family of *Caenorhabditis elegans* genes that can mutate to induce neuronal degeneration. Nature 349, 588–593.
Fire, A., Waterston, R.H., 1989. Proper expression of myosin genes in transgenic nematodes. EMBO J. 8, 3419–3428.
Halevi, S., McKay, J., Palfreyman, M., Yassin, L., Eshel, M., Jorgensen, E., Treinin, M., 2002. The *C. elegans ric-3* gene is required for maturation of nicotinic acetylcholine receptors. EMBO J. 21, 1012–1020.
Hamelin, M., Scott, I.M., Way, J.C., Culotti, J.G., 1992. The mec-7 beta-tubulin gene of Caenorhabditis elegans is expressed primarily in the touch receptor neurons. EMBO J. 11, 2885–2893.
Huang, M., Chalfie, M., 1994. Gene interactions affecting mechanosensory transduction in *Caenorhabditis elegans*. Nature 367, 467–470.
Hughes, C.L., Thomas, J.B., 2007. A sensory feedback circuit coordinates muscle activity in Drosophila. Mol. Cel. Neurosci. 35, 383–396.
Kaplan, J.M., Horvitz, H.R., 1993. A dual mechanosensory and chemosensory neuron in Caenorhabditis elegans. Proc. Natl Acad. Sci. USA 15, 2227–2231.
Kerr, R., Lev-Ram, V., Baird, G., Vincent, P., Tsien, R.Y., Schafer, W.R., 2000. Optical imaging of calcium transients in neurons and pharyngeal muscle of C. elegans. Neuron 26, 583–594.
Korta, J., Clark, D.A., Gabel, C.V., Mahadevan, L., Samuel, A.D., 2007. Mechanosensation and mechanical load modulate the locomotory gait of swimming C. elegans. J. Exp. Biol. 210, 2383–2389.
Li, W., Feng, Z., Sternberg, P.W., Xu, X.Z., 2006. A C. elegans stretch receptor neuron revealed by a mechanosensitive TRP channel homologue. Nature 440, 684–687.
Lumpkin, E.A., Caterina, M.J., 2007. Mechanisms of sensory transduction in the skin. Nature 445, 858–865.
Mitani, S., 1995. Genetic regulation of mec-3 expression implicated in the specification of the mechanosensory neuron cell types in Caenorhabditis elegans. Dev. Growth Diff. 37, 551–557.
Oren-Suissa, M., Hall, D.H., Treinin, M., Shemer, G., Podbilewicz, B., 2010. The fusogen EFF-1 controls sculpting of mechanosensory dendrites. Science 13, 861–868.
Sawin, E. R., 1996. Genetic and cellular analysis of modulated behaviors in Caenorhabditis elegans. PhD Thesis. Cambridge: MIT.
Sawin, E.R., Ranganathan, R., Horvitz, H.R., 2000. C. elegans locomotory rate is modulated by the environment through a dopaminergic pathway and by experience through a serotonergic pathway. Neuron 26, 619–631.
Smith, C.J., Watson, J.D., Spencer, W.C., O'Brien, T., Cha, B., Albeg, A., Treinin, M., Miller III, D.M., 2010. Time-lapse imaging and cell-specific expression profiling reveal dynamic branching and molecular determinants of a multi-dendritic nociceptor in C. elegans. Dev. Biol. 345, 18–33.
Suzuki, H., Kerr, R., Bianchi, L., Frokjaer-Jensen, C., Slone, D., Xue, J., Gerstbrein, B., Driscoll, M., Schafer, W.R., 2003. In vivo imaging of C. elegans mechanosensory neurons demonstrates a specific role for the MEC-4 channel in the process of gentle touch sensation. Neuron 39, 1005–1017.
Tavernarakis, N., Shreffler, W., Wang, S., Driscoll, M., 1997. unc-8, a DEG/ENaC family member, encodes a subunit of a candidate mechanically gated channel that modulates C. elegans locomotion. Neuron 18, 107–119.
Tracey, W.D., Wilson, R.I., Laurent, G., Benzer, S., 2003. *painless*, a *Drosophila* gene essential for nociception. Cell 113, 261–273.
Treinin, M., Chalfie, M., 1995. A mutated acetylcholine receptor subunit causes neuronal degeneration in *C. elegans*. Neuron 14, 871–877.
Treinin, M., Gillo, B., Liebman, L., Chalfie, M., 1998. Two functionally dependent acetylcholine subunits are encoded in a single Caenorhabiditis elegans operon. Proc. Natl Acad. Sci. USA 95, 15492–15495.
Tsalik, E.L., Niacaris, T., Wenick, A.S., Pau, K., Avery, L., Hobert, O., 2003. LIM homeobox gene-dependent expression of biogenic amine receptors in restricted regions of the C. elegans nervous system. Dev. Biol. 263, 81–102.
Waggoner, L.E., Tong Zhou, G., Schafer, R.W., Schafer, W.R., 1998. Control of alternative behavioral states by serotonin in *Caenorhabditis elegans*. Neuron 21, 203–214.
Watson, J.D., Wang, S., Von Stetina, S.E., Spencer, W.C., Levy, S., Dexheimer, P.J., Kurn, N., Heath, J.D., Miller III, D.M., 2008. Complementary RNA amplification methods enhance microarray identification of transcripts expressed in the C. elegans nervous system. BMC Genomics 9, 84.
Way, J.C., Chalfie, M., 1988. *mec-3*, a homeobox-containing gene that specifies differentiation of the touch receptor neurons in C. elegans. Cell 54, 5–16.
Way, J.C., Chalfie, M., 1989. The mec-3 gene of Caenorhabditis elegans requires its own product for maintained expression and is expressed in three neuronal cell types. Genes Dev. 1823–1833.
White, J.G., Southgate, E., Thomson, J.N., Brenner, S., 1986. The structure of the nervous system of the nematode *Caenorhabditis elegans*. Phil. Trans. R. Soc. B. 314, 1–340.
Yassin, L., Gillo, B., Kahan, T., Halevi, S., Eshel, M., Treinin, M., 2001. Characterization of the DEG-3/DES-2 receptor: a nicotinic acetylcholine receptor that mutates to cause neuronal degeneration. Mol. Cel. Neurosci. 17, 589–599.
Zhang, Y., Ma, C., Delohery, T., Nasipak, B., Foat, B.C., Bounoutas, A., Bussemaker, H.J., Kim, S.K., Chalfie, M., 2002. Identification of genes expressed in C. elegans touch receptor neurons. Nature 418, 331–335.
Zhang, M., Chung, S.H., Fang-Yen, C., Craig, C., Kerr, R.A., Suzuki, H., Samuel, A.D., Mazur, E., Schafer, W.R., 2008. A self-regulating feed-forward circuit controlling C. elegans egg-laying behavior. Curr. Biol. 18, 1445–1455.
Zhao, B., Khare, P., Feldman, L., Dent, J.A., 2003. Reversal frequency in Caenorhabditis elegans represents an integrated response to the state of the animal and its environment. J. Neurosci. 23, 5319–5328.

Please cite this article as: Albeg, A., et al., *C. elegans* multi-dendritic sensory neurons: Morphology and function, Mol. Cell. Neurosci. (2010), doi:10.1016/j.mcn.2010.10.001